Energy-Aware 3D Unmanned Aerial Vehicle Deployment for Network Throughput Optimization

Shih-Fan Chou, *Member, IEEE*, Ai-Chun Pang, *Senior Member, IEEE*, and Ya-Ju Yu, *Member, IEEE*

***Abstract*— Introducing mobile small cells to next generation cellular networks is nowadays a pervasive and cost-effective way to fulfill the ever-increasing mobile broadband traffic. Being agile and resilient, unmanned aerial vehicles (UAVs) mounting small cells are deemed emerging platforms for the provision of wireless services. As the residual battery capacity available to UAVs determines the lifetime of an airborne network, it is essential to account for the energy expenditure on various flying actions in a flight plan. The focus of this paper is therefore on studying the 3D deployment problem for a swarm of UAVs, with the goal of maximizing the total amount of data transmitted by UAVs. In particular, we address an interesting trade-off among flight altitude, energy expense and travel time. We formulate the problem as a non-convex non-linear optimization problem and propose an energy-aware 3D deployment algorithm to resolve it with the aid of Lagrangian dual relaxation, interior-point and subgradient projection methods. Afterwards, we prove the optimality of a special case derived from the convexification transformation. We then conduct a series of simulations to evaluate the performance of our proposed algorithm. Simulation results manifest that our proposed algorithm can benefit from the proper treatment of the trade-off.**

***Index Terms*— 3D deployment, cellular network, Lagrangian dual relaxation, maneuvering power, non-convex non-linear optimization, unmanned aerial vehicle (UAV).**

I. Introduction

THE massive increase in the number of mobile subscribers, connected devices and diverse network applications has driven an enormous growth in mobile data traffic, and a continuous surge in traffic demand will reach 49 exabytes per month by 2021 [1]. Current cellular networks therefore require deploying additional base stations to accommodate such voluminous amounts of data [2]. One cost-saving and energy-effective approach is to employ mobile small cells for achieving ubiquitous coverage and capacity [3], [4]. Particularly, a growing interest in the aerial provision of communication services creates an innovative network paradigm. Flying base stations (FBSs) with small cells mounted on airborne vehicles are pervasively used in a variety of application domains [5], such as in unexpected or temporary environments. In view of this, several projects have been under development. To deliver universal network connectivity, Google Loon Project [6] has conducted airborne communications using balloons to complement the existing terrestrial wired/wireless infrastructure. Also, ABSOLUTE FP7 European Project [7] has built a hybrid 3GPP LTE-A land-and-air architecture which offers coverage/capacity enhancement in an agile fashion in cases such as public safety communications or during extreme and temporary events. As a result, FBSs are deemed as potential new technologies in future cellular networks.

Being stable and controllable [8], unmanned aerial vehicles (UAVs) flying autonomously or being piloted remotely without carrying any human staff are now common airborne carriers with the following benefits. As mobility is a salient feature, UAVs can freely move to favorable places in 3D space[1] to construct airborne networks in a quick and flexible manner. Scenarios such as inaccessible and dangerous areas out of reach of conventional terrestrial base stations thus can keep network connectivity. In addition to adapt to versatile network topologies, the capability of tracking regions of interest also enables on-demand communications. UAVs therefore can assist existing network infrastructures in extending coverage and capacity as well as relieving mobile data traffic, especially for high-demand or overloaded areas. Furthermore, the degree of freedom in flight altitude brings a higher chance of maintaining line-of-sight (LoS) communications, thus increasing the quality of service (QoS) offered to users.

Despite the merits mentioned above, UAVs powered by batteries suffer from low energy capacity. As the limited energy supply constrains the network lifetime, a larger energy loss

Manuscript received October 1, 2018; revised March 30, 2019 and July 28, 2019; accepted September 25, 2019. Date of publication October 17, 2019; date of current version January 8, 2020. The work of A.-C. Pang was supported in part by the Ministry of Science and Technology under Grant 108-2221-E-002-069-MY3, Grant 107-2923-E-002-006-MY3, and Grant 106-2221-E-002-MY2, in part by the National Taiwan University under Grant 108L880503, in part by the Ministry of Economic Affairs under Grant 107-EC-17-A-02-S5-007, in part by MOXA, and in part by Microsoft Research Asia. The work of Y.-J. Yu was supported in part by the Ministry of Science and Technology under Grant 107-2218-E-390-003-MY3. The associate editor coordinating the review of this article and approving it for publication was M. Li. *(Corresponding author: Ai-Chun Pang.)*

S.-F. Chou is with the Research Center for Information Technology Innovation (CITI), Academia Sinica, Taipei 115, Taiwan (e-mail: sfchou@citi.sinica.edu.tw).

A.-C. Pang is with the Graduate Institute of Networking and Multimedia, Department of Computer Science and Information Engineering, National Taiwan University, Taipei 106, Taiwan, and also with the Research Center for Information Technology Innovation (CITI), Academia Sinica, Taipei 115, Taiwan (e-mail: acpang@csie.ntu.edu.tw).

Y.-J. Yu is with the Department of Computer Science and Information Engineering, National University of Kaohsiung, Kaohsiung 811, Taiwan (e-mail: yjyu@nuk.edu.tw).

Color versions of one or more of the figures in this article are available online at http://ieeexplore.ieee.org.

Digital Object Identifier 10.1109/TWC.2019.2946822

[1]Compared to the 2D space, a 3D space adding a dimension in the z-direction is the Euclidean space that maps with an xyz coordinate system.

1536-1276 © 2019 IEEE. Personal use is permitted, but republication/redistribution requires IEEE permission.
See http://www.ieee.org/publications_standards/publications/rights/index.html for more information.

Authorized licensed use limited to: Korea Univ. Downloaded on February 13,2020 at 05:48:36 UTC from IEEE Xplore. Restrictions apply.

will result in a shorter life expectancy of an airborne network. To truly reveal the efficacy of the UAV deployment, the energy expenses in a flight should be well-planned. Typically, radio communication power and maneuvering power are two major energy consumers prerequisite to the provision of Internet data services and the sustenance of mechanical activities of UAVs,[2] with average energy consumption of a few watts and hundreds of watts [9], respectively. To conform with the realistic condition, the design of 3D deployment needs to simultaneously consider both radio communication power and maneuvering power.

In this paper, we study the 3D UAV deployment problem, aiming at maximizing the total amount of data transmitted by UAVs while mitigating the co-tier interference among them. Below are our contributions.

- *Main observation*: A trade-off pertaining to the maximization of the amount of data is outlined among the travel time, the flight altitude and the battery lifetime of each UAV. Based on this observation, the 3D deployment is formulated as a non-convex non-linear optimization program, followed by the design of a deployment algorithm to properly determine the 3D location of each UAV.
- *Problem transformations and optimal solution*: Owing to the non-convexity and non-linearity, the initially formulated problem is intractable and hard to solve directly. We then derive the corresponding convexified linear transformation of the optimization problem, which is a special case to provide a good approximation to the original one, and prove its optimality.
- *Validation and evaluation*: We perform a series of simulations to evaluate the performance of the proposed algorithm and give in-depth insights into the 3D deployment problem.

The remainder of this paper is organized as follows. Section II briefly reviews the related works on UAV deployment. Section III presents the system model and problem formulation. In Section IV, we develop a 3D deployment algorithm and derive an optimal solution for a special case. In Section V, we discuss technical implementation issues that arise with the proposed algorithm in next-generation cellular systems. Simulation results and analyses are drawn and discussed in Section VI. Eventually, Section VII concludes the paper.

II. Related Work

Recently, the exploitation of UAVs has attracted significant attention from both academia and industry [10]. In order to reveal the benefits of UAVs, a proper decision on the deployment plan should be made in advance. A number of literatures have dedicated to the deployment problem from the viewpoints of diverse performance measures and can be generally categorized into three classes in terms of deployment flexibility. The first category, referred to as 1D deployment, merely focuses on exploring the influence of flight altitudes. Al-Hourani *et al.* [11] presented an analytical model that attempts to locate a single low-altitude aerial platform (LAP) at the optimal altitude such that the radio coverage on the ground is maximized. Mozaffari *et al.* [12] determined the optimal altitude for a single drone small cell (DSC) to simultaneously maximize ground coverage and minimize required transmit power, followed by the investigation of the optimal distance relationship between two DSCs in interference-free and interference situations.

The second category, viewed as 2D deployment, considers the placement problem at a given altitude in horizontal space without characterizing the air-to-ground channels. The mobility behavior of UAVs in [13] followed from the virtual potential fields that employ the information of distance and RSSI to strike an optimal balance between ground area coverage and ground service provisioning time. Lyu *et al.* [14] proposed a spiral algorithm to deploy the minimum number of UAVs so that each user is within the coverage of at least one UAV. Merwaday *et al.* [15] used a genetic algorithm to maximize the fifth-percentile throughput for cell-edge users under the scenarios of public-safety communications.

In fact, the performance gains from UAV deployment depend on both flight altitudes and positions on the xy plane. To address the issue, the third category, regarded as 3D deployment, usually decouples the deployment problem into subproblems that involve vertical and horizontal dimensions. Bor-Yaliniz *et al.* [16] and Bor-Yaliniz and Yanikomeroglu [17] formulated the 3D deployment as a mixed integer non-linear programming problem with the objective of maximizing the number of served users with the minimum required area. To consider network deployment costs, Kalantari *et al.* [18] further adopted particle swarm optimization algorithm to decide the minimum number of drone base stations and the suboptimal 3D placement while satisfying QoS requirements of all users. Helmy *et al.* [19] designed a dynamic placement and sizing algorithm to achieve load balancing and improve network throughput. In [20], Kalantari *et al*. studied the impact of different types of wireless backhaul on the network coverage performance in both network-centric and user-centric approaches. Alzenad *et al.* [21] and Mozaffari *et al.* [22] devised optimal placement mechanisms to maximize the total coverage using the minimum transmit power while extending the coverage lifetime. To achieve the fairness among users, Wu *et al.* [23] aimed at maximizing the minimum throughput over all users by jointly optimizing the multi-user scheduling and association, UAV trajectories, and the power control. In [24] and [25], Shi *et al*. respectively investigated the 3D multi-drone-cell (multi-DC) trajectory planning and scheduling approach under the scenarios of IoT data collection and drone assisted radio access networks to minimize the average user-to-DC path loss. Chen *et al.* [26], [27] introduced cache-enabled UAVs to the 3D deployment. To maximize users' QoE requirements with the minimum transmit power, the work in [26] exploited the conceptor-based echo state network learning algorithm to predict users' content request distribution and mobility patterns. In [27], a liquid state machine learning algorithm is developed to maximize the number of stable queue users. However, all the above researches only concentrated on the transmit power without considering

[2]Climb up and down, move in a straight direction and hover at a point are universally the most common basic operations performed by UAVs.

Authorized licensed use limited to: Korea Univ. Downloaded on February 13,2020 at 05:48:36 UTC from IEEE Xplore. Restrictions apply.

the maneuvering power. As maneuvering operations expend most energy deposits in a deployment plan, purely discussion on the transmit power cannot fully describe the 3D deployment problem. Hence, none of the above-mentioned related works offers a holistic solution for coping with the trade-off among flight altitude, travel time and battery lifetime of UAVs yet.

To address the above trade-off issue, Chou *et al.* [28] investigated the 3D deployment strategy for a swarm of aerial small cells (ASCs) with the purpose of maximizing the total throughput of all users within limited lifetime budgets. A heuristic algorithm to the general energy-aware 3D ASC deployment problem was developed and the received data rates of users were measured by several modulation and coding schemes assuming a specific symbol rate. In this paper, we dedicate to the theoretical derivation of the 3D deployment problem and calculate the data rate by using a popular air-to-ground channel model to characterize the uniqueness of channels suitable for 3D urban environments. In addition, we further delve into a special case where the convexification technique is employed to provide a good approximation to the original intractable problem, followed by the proof of its optimality.

III. System Model and Problem Formulation

This section sketches broad outlines of our energy-aware 3D UAV deployment problem. The intrinsic mobility makes UAVs capable of tracking the user dynamics in time and space, thus bringing the supply to where the traffic demand is. To truly profit from the mobility capability, it is crucial to take an appropriate flight planning and the details are elaborated in Subsection III-A. Subsection III-B presents the air-to-ground channel model used for calculating received data rates. We consider an urban scenario for better capacity and therefore adopt here the one specialized in urban environments among currently available channel models [11], [29]. Finally, Subsection III-C formulizes our energy-aware 3D UAV deployment problem.

A. System Model

We consider a two-tier network structure in which a swarm of UAVs equipped with small cells is overlaid over macrocells. Each UAV powered by batteries can dynamically move from one place to another to provide communication services for users in high traffic load areas or in densely populated areas. A land-based entity, called the ground control station (GCS), controls and manages UAVs from any remote place. Owing to the mobility of UAVs, wireless backhaul technologies such as high-rate millimeter wave or high-capacity free-space optics (FSO) [20], [30] are utilized to transport traffic from UAVs to the GCS. Then the GCS and macrocells are backhaul-connected to the core network using wired technologies (e.g., fiber). Fig. 1 depicts an illustrative paradigm of the system. Our aim is to find the 3D deployment of UAVs such that the total amount of data transmitted by UAVs within the limited network lifetime is maximized. To properly determine the target location for each UAV, three factors vital to the 3D

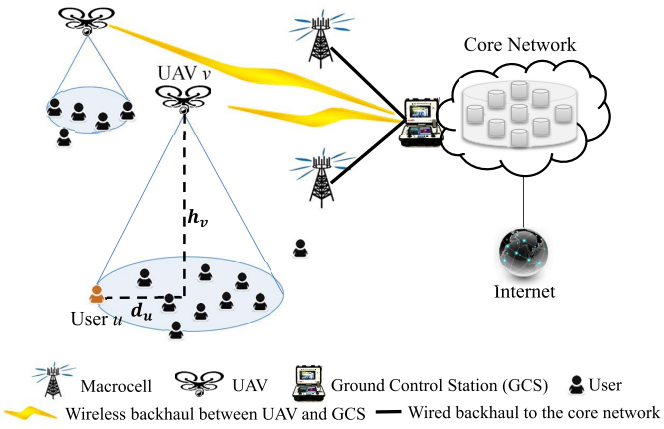

Fig. 1. System overview.

deployment should be took into account simultaneously: flight altitude, energy consumption and available lifetime. To begin with, how to leverage the mobility ability of each UAV to find its favorable flight altitude is critical. When a UAV flies at a high altitude, the ground coverage expands at the cost of weaker signal strength. Conversely, a UAV flying at a low altitude enables stronger signal strength, whereas the ground coverage shrinks. In fact, the power of a radio signal weakens as a square of distance according to the communication features [31] and a large coverage area usually allows more served users. The trade-off is that each UAV should fly at a high altitude to serve a larger number of users with lower signal quality or fly at a low altitude to serve a fewer number of users with higher signal quality. As envisioned, the more users being supplied with good signal quality, the higher the chance to facilitate the total amount of data. On the other hand, another trade-off exists between the throughput and the lifetime of each UAV. A UAV flying towards a high-throughput but distant place inclines to expend considerable amounts of energy, leading to a short lifetime in the air. In contrast, although a UAV flying towards a nearby place can save energy for a longer lifetime, the place may contribute little to the throughput. Since signals will experience severe fading in the flight duration, UAVs are supposed to delay services until arriving at their target locations and the users it originally served might associate with a corresponding macrocell for service continuity. It is then quite apparent that a longer flight time will incur a larger loss in both the service time and the amount of data. In general, it will be beneficial for the total amount of data if each UAV can serve as many users as possible with excellent signal quality for a long period of time. Notice that a UAV will preserve enough power in advance to return back to the ground for recharge before running out of energy. In addition, each user will only choose to connect with either the macrocell or a UAV with the most strengthened signal quality. Without loss of generality, our proposed algorithm can accommodate any kind of well-developed user association techniques and bandwidth allocation mechanisms. To deal with the dependency relationship among user association, bandwidth allocation, and optimal location selection of UAVs, this paper exploits an iterative search method to

Authorized licensed use limited to: Korea Univ. Downloaded on February 13,2020 at 05:48:36 UTC from IEEE Xplore. Restrictions apply.

determine the optimal locations with the highest total amount of data. As mentioned in [32], since the continuous tracking of users will incur a high cost to battery-powered UAVs, the position of a UAV is often fixed at a location at least for a minimum period of time. Once the user location prediction is done, this paper deploys UAVs without change in a time interval.

B. Air-to-Ground Channel Model

Since there is a higher chance of delivering LoS connectivity, air-to-ground channel characterization is quite distinct from the terrestrial channels. A popular approach to model air-to-ground communications in urban environments is to classify the propagated signals into LoS and non-LoS (NLoS) groups. Given a transmit power P_t, a ground user u located d_u horizontal distance from its serving UAV v at flight altitude of h_v will receive a signal power of strength

$$P_t - L_{h_v,d_u} \tag{1}$$

where L_{h_v,d_u} represents the path loss a radio signal propagated through a wireless medium, which is the average over LoS and NLoS connections:

$$L_{h_v,d_u} = p_l \times L_l + p_n \times L_n \tag{2}$$

p_l and p_n are respectively probabilities of LoS and NLoS connections between a UAV and a ground user, calculated as [11]

$$p_l = \frac{1}{1 + a \cdot e^{-b\left[tan^{-1}\left(\frac{h_v}{d_u}\right) - a\right]}} \tag{3a}$$

$$p_n = 1 - p_l \tag{3b}$$

where a and b are constant values determined by the environment (e.g., urban, rural). $tan^{-1}\left(\frac{h_v}{d_u}\right)$ indicates the elevation angle in radian between UAV v and ground user u. Besides, the average path losses for both LoS and NLoS connections in dB can be expressed as

$$L_l = 20log\left(\frac{4\pi f\sqrt{h_v^2 + d_u^2}}{c}\right) + \epsilon_l \tag{4a}$$

$$L_n = 20log\left(\frac{4\pi f\sqrt{h_v^2 + d_u^2}}{c}\right) + \epsilon_n \tag{4b}$$

where the first terms of Equation (4a) and (4b) stand for the free space path loss between a UAV and a ground receiver. Variable f is the carrier frequency, c is the speed of light, ϵ_l and ϵ_n are the average additional losses to the free space propagation loss.

Substituting Equations (3a), (3b), (4a) and (4b) into Equation (2) yields the following result:

$$\begin{aligned} L_{h_v,d_u} &= p_l \times L_l + p_n \times L_n \\ &= \frac{\epsilon_l - \epsilon_n}{1 + a \cdot e^{-b\left[tan^{-1}\left(\frac{h_v}{d_u}\right) - a\right]}} \\ &\quad + 20log\left(\frac{4\pi f\sqrt{h_v^2 + d_u^2}}{c}\right) + \epsilon_n \end{aligned}$$

C. Problem Formulation

In this paper, we study the 3D deployment problem of a fleet of UAVs over next-generation cellular networks. Given that the user distribution is known and that every UAV has finite battery life, our objective aims at maximizing the total amount of data transmitted by UAVs. The following formulates the system model. In the network, there is a set of users $\mathcal{U}$ waiting for services. Each user u occupies a location (x_u, y_u) on the coordinate plane and all users are assumed to have the same dwell time. Let $\mathcal{V}$ be a swarm of UAVs. Each UAV v flying in 3D free space has an available bandwidth of B_v MHz and an available energy budget of E_v kJ. Also, the transmit power of a UAV is P_t. Compared with radio communications, maneuvering operations that support for the essential mechanics consume a major portion of the total energy input. Typically, climb, move and hover are three common types of actions involved in a flight, and each of which consumes an average power of P_c, P_m and P_h Watts. Every flight between any two locations could be accomplished by a combination of a series of actions. For instance, a UAV may first take $t_{h_v \to h'_v}$ time to climb from height h_v to height h'_v, followed by $t_{(x_v,y_v)\to(x'_v,y'_v)}$ time of the horizontal movement from position (x_v, y_v) to position (x'_v, y'_v). After travelling from start location l_v to target location l'_v, UAV v hovers in situ for a period of time $t_{l_v \to l'_v}$ and supplies a set of users $\mathcal{U}_{l'_v}$ with services. Here, $l_v = (x_v, y_v, h_v)$ is a 3D coordinate, indicating the position on the *xy* plane and the height in *z*-direction. $t_{l_v \to l'_v} = \max\left\{0, \frac{E_v - P_m t_{(x_v,y_v)\to(x'_v,y'_v)} - P_c t_{h_v \to h'_v}}{P_h + P_t}\right\}$ computes the service time of a user limited to the energy deposit of its serving UAV. Based on the Shannon capacity theory, user $u \in \mathcal{U}_{l'_v}$ serving by UAV v at location l'_v will enjoy a data rate of r_{u,l'_v}:

$$r_{u,l'_v} = b_{v,u} \cdot log_2\left(1 + \frac{P_t - L_{h'_v,d_u}}{\sum_{\forall w \in \mathcal{V}, w \neq v}(P_t - L_{h'_w,d_u}) + N}\right)$$

where $b_{v,u}$ indicates the amount of bandwidth allocated to user u by UAV v and each UAV is assumed to equally distribute its available bandwidth B_v among its associated users. Note that our paper can adopt one of the existing bandwidth allocation mechanisms for the 3D deployment. N is the average power of the noise and interference over the bandwidth. To mitigate the co-tier interference and reduce the coverage overlap, the inter-UAV distance between any pair of UAVs is at least D. The 3D deployment is often executed by a central server at the start of a flight plan and is feasible if fulfilling the following constraints:

1) UAV Energy Capacity: Equation (5) ensures that the total energy consumed by UAV v within its lifetime does not surpass its available energy budget E_v.

$$P_m t_{(x_v,y_v)\to(x'_v,y'_v)} + P_c t_{h_v \to h'_v} + (P_h + P_t) t_{l_v \to l'_v} \leq E_v, \quad \forall v \in \mathcal{V}, l'_v \tag{5}$$

2) Minimum Inter-UAV Distance Requirement: When UAVs become ready for service provision at their target locations, the interference-free distance between any two distinct UAVs

Authorized licensed use limited to: Korea Univ. Downloaded on February 13,2020 at 05:48:36 UTC from IEEE Xplore. Restrictions apply.

should be greater than or equal to a minimum value D so as to reduce the influence of co-tier interference as well as decrease the possibility of coverage overlap.

$$\sqrt{(x'_v - x'_w)^2 + (y'_v - y'_w)^2} \geq D, \quad \forall v, w \in \mathcal{V}, v \neq w \quad (6)$$

3) Flight Altitude Constraint: This constraint expresses that the final altitude of each UAV must be between certain maximum and minimum allowed values in order to comply with the flying regulations [33].

$$\bar{A} \leq h'_v \leq A, \quad \forall v \in \mathcal{V} \quad (7)$$

4) Bandwidth Resource Constraint: For any UAV v, the total amount of bandwidth used to serve the ground users cannot exceed its available bandwidth unit B_v.

$$\sum_{\forall u \in \mathcal{U}_{l'_v}} b_{v,u} \leq B_v, \quad \forall v \in \mathcal{V}, l'_v \quad (8)$$

The Energy-Aware 3D Unmanned Aerial Vehicle Deployment Problem

Input instance: Given a user set $\mathcal{U}$. Each user u located at (x_u, y_u) is always assumed to be ready to receive services. There is a set of UAVs $\mathcal{V}$. Each UAV v powered by batteries with transmit power P_t has an available bandwidth B_v and an available energy budget E_v. Due to the safety consideration, every flight should keep an altitude between $\bar{A}$ and A in the air. When setting out a journey from the start location $l_v = (x_v, y_v, h_v)$ to the target location $l'_v = (x'_v, y'_v, h'_v)$, UAV v may experience a horizontal travel time $t_{(x_v,y_v)\to(x'_v,y'_v)}$ and a vertical travel time $t_{h_v \to h'_v}$ individually. After reaching target location l'_v, UAV v eventually hovers at that point and then provides services to a set of users $\mathcal{U}_{l'_v}$ within its residual lifetime. Climb, move and hover are three potential actions during a flight and will respectively consume an average power of P_c, P_m and P_h Watts. D is a parameter for setting the minimum interference-free distance among UAVs.

Output instance: When locating the target position l'_v for each UAV v, the corresponding data rate r_{u,l'_v} of each user u and the service time $t_{l_v \to l'_v}$ experienced by each UAV v are determined.

Objective: Our objective is to find a proper target location l'_v for each UAV v in 3D space such that the total amount of data transmitted by UAVs is maximized. The following expression formalizes the objective function.

$$\max_{l'_v} \sum_{\forall v \in \mathcal{V}} \sum_{\forall u \in \mathcal{U}_{l'_v}} r_{u,l'_v} \cdot t_{l_v \to l'_v} \quad (9)$$

subject to the constraints (5) to (8). Table I summarizes the notations used throughout the paper.

TABLE I
SUMMARY OF NOTATIONS

Symbol	Description
$\mathcal{V}$	The set of UAVs
$\mathcal{U}$	The set of users
$\mathcal{U}_{l'_v}$	The set of users served by UAV v at target location l'_v, where $l'_v = (x'_v, y'_v, h'_v)$
r_{u,l_v}	The data rate of user u provided by its serving UAV v at location l_v
$t_{(x_v,y_v)\to(x'_v,y'_v)}$	The horizontal movement time for UAV v from position (x_v, y_v) to position (x'_v, y'_v)
$t_{h_v \to h'_v}$	The vertical movement time for UAV v from altitude h_v to altitude h'_v
$t_{l_v \to l'_v}$	The service time for a user provided by its serving UAV v after travelling from start location l_v to target location l'_v
A	The maximum flight altitude of a UAV
$\bar{A}$	The minimum flight altitude of a UAV
P_c	Power consumed by a UAV in climbing
P_m	Power consumed by a UAV during movement
P_h	Power consumed by a UAV when hovering
P_t	Transmit power of a UAV
E_v	Available energy budget of UAV v
B_v	Available bandwidth to UAV v
$b_{v,u}$	The amount of bandwidth allocated to user u by UAV v
D	The minimum inter-UAV distance

IV. ENERGY-AWARE 3D UNMANNED AERIAL VEHICLE DEPLOYMENT

In this section, we are committed to tackling the energy-aware 3D unmanned aerial vehicle deployment problem. First of all, the Lagrangian method is applied to transform the optimization problem into an equivalent dual problem, which can be solved by the subgradient projection method. Next, we propose a general heuristic algorithm, called *Energy-Aware 3D UAV Deployment (EAUD)* algorithm, to properly settle UAVs in 3D space. We then focus on a special case by reformulating the non-convex optimization problem to a convex one and eventually derive its optimality.

A. Lagrangian Dual Relaxation

For a non-convex non-linear program, it is often difficult to find a closed form for a function being maximized or minimized. One of the potential ways to efficiently deal with this class of problems is the use of the Lagrangian method [34]. Being a powerful tool without the need for explicitly solving the constraints of the problems, the Lagrangian method can be used to derive easily solvable problems for the approximate optimal solutions by eliminating extra variables. Therefore, each non-convex non-linear function/constraint is replaced with a looser, but convex linear function/constraint. In view of this, we adopt the Lagrangian method to solve the non-convex non-linear optimization problem (9). Relaxing both UAV energy capacity (5) and the minimum inter-UAV distance (6) constraints by adding the objective function with a weighted sum of constraints will introduce the following Lagrangian function.

$$\begin{aligned}\mathcal{L}(\boldsymbol{l'}, \boldsymbol{\lambda}, \boldsymbol{\rho}) = & \sum_{\forall v \in \mathcal{V}} \sum_{\forall u \in \mathcal{U}_{l'_v}} r_{u,l'_v} \cdot t_{l_v \to l'_v} \\ & + \sum_{\forall v \in \mathcal{V}} \lambda_v \Big(E_v - P_m t_{m_v \to m'_v} - P_c t_{h_v \to h'_v} \\ & \qquad - (P_h + P_t) t_{l_v \to l'_v} \Big) \\ & + \sum_{\forall v \in \mathcal{V}} \sum_{\forall w \in \mathcal{V}, w \neq v} \rho_{vw} \big(\|m'_v - m'_w\|_2 - D \big)\end{aligned}$$

Authorized licensed use limited to: Korea Univ. Downloaded on February 13,2020 at 05:48:36 UTC from IEEE Xplore. Restrictions apply.

where $\boldsymbol{l'} = \{(x'_v, y'_v, h'_v) | v \in \mathcal{V}\}$ is the coordinate vector of UAVs in 3D space. The weights $\boldsymbol{\lambda} = \{\lambda_v | v \in \mathcal{V}\}$ and $\boldsymbol{\rho} = \{\rho_{vw} | v, w \in \mathcal{V}, v \neq w\}$ associated with constraints (5) and (6) are referred to as Lagrange multiplier vectors, indicating the energy gains and interference gains from UAVs.

Let $m_i = (x_i, y_i)^T \in \Re^2$ be the 2D horizontal coordinate of UAV i and $\|\cdot\|_2$ be the Euclidean norm (or l_2 norm). Combined with the transpose operation $(\cdot)^T$ on given vectors, we get

$$\begin{aligned} \|m'_v - m'_w\|_2 &= \sqrt{(m'_v - m'_w)^T (m'_v - m'_w)} \\ &= \sqrt{(x'_v - x'_w, y'_v - y'_w)(x'_v - x'_w, y'_v - y'_w)^T} \\ &= \sqrt{(x'_v - x'_w)^2 + (y'_v - y'_w)^2} \end{aligned}$$

which is equivalent to the left-hand side of inequality (6).

The Lagrange dual function is defined as the maximum value of the Lagrangian over $\boldsymbol{l'}$:

$$g(\boldsymbol{\lambda}, \boldsymbol{\rho}) = \max_{\boldsymbol{l'}} \mathcal{L}(\boldsymbol{l'}, \boldsymbol{\lambda}, \boldsymbol{\rho}) \tag{10}$$

Also, the Lagrange dual problem corresponding to the primal problem (9) is written as the following optimization problem.

$$\min\ g(\boldsymbol{\lambda}, \boldsymbol{\rho}) \tag{11}$$

subject to

$$\boldsymbol{\lambda} \succeq \boldsymbol{0}, \quad \boldsymbol{\rho} \succeq \boldsymbol{0} \tag{12}$$

B. General Solution Method

To solve the dual problem (11), we apply the subgradient projection method [35] that generates minimizing sequences of dual variables iteratively:

$$\lambda_v(k+1) = \left[\lambda_v(k) - \beta(k) \frac{\partial g(\boldsymbol{\lambda}(k), \boldsymbol{\rho}(k))}{\partial \lambda_v(k)}\right]^+ \tag{13}$$

$$\rho_{vw}(k+1) = \left[\rho_{vw}(k) - \beta(k) \frac{\partial g(\boldsymbol{\lambda}(k), \boldsymbol{\rho}(k))}{\partial \rho_{vw}(k)}\right]^+ \tag{14}$$

where k is the iteration index, $[\alpha]^+ = \max\{0, \alpha\}$ and $\beta(k) > 0$ is the step size at iteration k. Here, $\beta(k)$ is set as $0.5/k$ and the subgradient algorithm is guaranteed to converge to a dual optimal solution if the step sizes satisfy the diminishing step size rules:

$$\lim_{k \to \infty} \beta(k) = 0, \quad \sum_{k=1}^{\infty} \beta(k) = \infty$$

C. Energy-Aware 3D UAV Deployment Algorithm

This section designs an *Energy-Aware 3D UAV Deployment (EAUD)* algorithm to maximize the total amount of data transmitted by UAVs. Since the total amount of data highly depends on the flight altitude, the energy depletion and the available lifetime, a UAV spending considerable amounts of time hovering at its target location and offering more users with better data rates will induce a higher total amount of data. Our algorithm therefore tries to navigate each UAV towards its target location where contributes the most to the total amount of data without severe interference. *EAUD* will eventually terminate when all UAVs are in place by iteratively employing the subgradient projection [35] and interior-point [34] methods.

Algorithm 1 exhibits the pseudo code of the proposed *EAUD* approach. After completing the steps in Lines 1-25, each UAV v will locate itself at a target location with the maximum total amount of data. In Line 1, variable k with initial value of 0 is used to count the accumulated number of iterations. For each UAV v, variable δ_v, initialized as 0, $\forall v$ is used to record the relative difference in problem (10) between two consecutive iterations (Line 2). τ in the conditional statement on Line 3 is the predetermined maximal number of iterations that controls the algorithmic performance and convergence speed. The calculation procedure will persist until either all UAVs find their target locations or the number of iterations executed reaches the upper limit τ. Let "Flag" be an indicator that is TRUE if target locations are well-prepared for each UAV and FALSE otherwise. The initial value of "Flag" is TRUE, which means the existence of a full arrangement for all UAVs (Line 4). In the k-th iteration, we first apply the subgradient projection method in Equation (13) to update Lagrange multipliers $\lambda_v(k+1), \forall v$ (Line 6), followed by the update of Lagrange multipliers $\rho_{vw}(k+1), \forall v, w \in \mathcal{V}, v \neq w$, as in Equation (14) (Lines 7-9). Then, the horizontal movement time $t_{(x_v, y_v) \to (x'_v, y'_v)}(k+1)$, the vertical movement time $t_{h_v \to h'_v}(k+1)$ and the service time $t_{l_v \to l'_v}(k+1)$ can be computed using interior-point method based on the latest Lagrange multipliers, thus solving the non-convex optimization problem (10) (Line 10). We then evaluate the difference in values for each UAV v between the k-th and the $(k+1)$-th iterations and store the refreshed value in variable δ_v (Line 11). If all of the difference values are below the tolerance threshold η (i.e., Flag = TRUE), the algorithm will be terminated and the optimal solution will be output (Lines 13-24). Once confirming the target location $l'_v, \forall v$ (Line 21), each UAV v then takes $t_{(x_v, y_v) \to (x'_v, y'_v)}(k+1)$ and $t_{h_v \to h'_v}(k+1)$ time to fly from the original location l_v towards its target location l'_v in horizontal and vertical directions individually. Afterward *EAUD* returns the updated target location l'_v of each UAV $v, \forall v \in \mathcal{V}$ (Line 26). Otherwise, any violation of the tolerance threshold η (i.e., Flag = FALSE) will make *EAUD* enter the next iteration and repeat the above calculation process.

Theorem 1: The time complexity of Algorithm 1 is $O\left(\tau\left(|\mathcal{V}|(\varphi|\mathcal{V}| + \varepsilon) + |\mathcal{V}|\right)\right)$.

Proof: For the first inner **for** loop (Lines 5-12), we apply the subgradient projection method to update Lagrange multiplier λ_v for each UAV v and Lagrange multiplier ρ_{vw} between UAV v and any other UAV w, respectively. In other words, each UAV will update Lagrange multiplier at most $|\mathcal{V}|$ times. With the aid of the latest Lagrange multipliers, the optimization problem can then be solved by the interior-point method. Given that φ and ε are the time complexities of the subgradient projection method and the interior-point method, this process for one UAV overall takes $O(\varphi|\mathcal{V}| + \varepsilon)$ time. Since there are at most $|\mathcal{V}|$ UAVs, the time complexity of the **for** loop is $O(|\mathcal{V}|(\varphi|\mathcal{V}| + \varepsilon))$. For the second inner **for** loop (Lines 13-18), it takes $O(|\mathcal{V}|)$ time to check whether an

Authorized licensed use limited to: Korea Univ. Downloaded on February 13,2020 at 05:48:36 UTC from IEEE Xplore. Restrictions apply.

Algorithm 1 Energy-Aware 3D Unmanned Aerial Vehicle Deployment

Input: $\mathcal{U}, \mathcal{V}, l_v, \mathcal{U}_{l'_v}, A, \bar{A}, P_c, P_m, P_h, E_v, B_v, D, \tau, \eta$
Output: $l'_v, \forall v \in \mathcal{V}$
1: $k \leftarrow 0$
2: $\delta_v \leftarrow 0, \forall v$
3: **for** $k \leq \tau$ **do**
4: Flag $\leftarrow$ TRUE
5: **for all** $v \in \mathcal{V}$ **do**
6: Update Lagrange multiplier $\lambda_v(k+1)$ using the subgradient projection method, as in (13)
7: **for all** $w \in \mathcal{V}, w \neq v$ **do**
8: Update Lagrange multiplier $\rho_{vw}(k+1)$ using the subgradient projection method, as in (14)
9: **end for**
10: Calculate $t_{(x_v,y_v)\rightarrow(x'_v,y'_v)}(k+1)$, $t_{h_v\rightarrow h'_v}(k+1)$ and $t_{l_v\rightarrow l'_v}(k+1)$ by utilizing interior-point method with $\lambda_v(k+1)$ and $\rho_{vw}(k+1), \forall v, w \in \mathcal{V}, v \neq w$ to solve problem (10)
11: Estimate and renew the difference value δ_v of problem (10) between the k-th and the $(k+1)$-th iterations
12: **end for**
13: **for** $v = 1 \rightarrow |\mathcal{V}|$ **do**
14: **if** $\delta_v > \eta$ **then**
15: Flag $\leftarrow$ FALSE
16: Break the **for** loop
17: **end if**
18: **end for**
19: **if** Flag = TRUE **then**
20: **for all** $v \in \mathcal{V}$ **do**
21: $l'_v \leftarrow (x'_v(k+1), y'_v(k+1), h'_v(k+1))$
22: **end for**
23: Break the **for** loop
24: **end if**
25: **end for**
26: **return** $l'_v, \forall v \in \mathcal{V}$

optimal solution is found for each UAV. If confirming the optimal solutions, the third inner **for** loop (Lines 20-22) takes $O(|\mathcal{V}|)$ time to locate each UAV to its target location. Since the above procedures may be carried out at most τ times (i.e., the outer **for** loop (Lines 3-25)), the time complexity of Algorithm 1 is $O\left(\tau\left(|\mathcal{V}|(\varphi|\mathcal{V}|+\varepsilon)+|\mathcal{V}|\right)\right)$. ■

D. Special Case - Convexified Optimization Problem

Due to the non-convexity and non-linearity of constraint (6), the formulated optimization problem (9) is non-convex and non-linear regardless of the convexity and linearity of the objective function and other constraints and therefore falls into the category of non-convex non-linear programs, which are in general hard to solve [36], [37]. To make the problem-solving process more tractable and effective, we investigate the special case where the convexification technique is employed to provide a good approximation to the original problem. Proposition 1 demonstrates the transformation of the non-convex non-linear program into a restricted convex linear one.

Proposition 1: Let $\boldsymbol{m} = \{m_1, m_2, \cdots, m_{|\mathcal{V}|}\}$ *be a set of vectors, where* $m_i = (x_i, y_i)^T \in \Re^2$ *represents the 2D horizontal coordinate of UAV* i*. For any pair of UAVs, a convex restriction of the non-convex minimum inter-UAV distance constraint* $\|m_i - m_j\|_2 \geq D, \forall i, j \in \mathcal{V}, i \neq j$ *can be formed as* $q_{i,j}^T(m_i - m_j) \geq D$*, where* $q_{ij} \in \Re^2$ *and* $\|q_{ij}\|_2 = 1, \forall i, j \in \mathcal{V}, i < j$.

Proof: Assume that $\widehat{\mathbf{m}} = \{\widehat{m_1}, \widehat{m_2}, \cdots, \widehat{m_{|\mathcal{V}|}}\}$ is an approximate solution. We can set $q_{ij} = \frac{\widehat{m_i} - \widehat{m_j}}{\|\widehat{m_i} - \widehat{m_j}\|_2} \in \Re^2$, for $i < j, \forall i, j \in \mathcal{V}$ such that $\|q_{ij}\|_2 = 1$.

Follows immediately from Cauchy-Schwarz inequality, we have:

$$\|m_i - m_j\|_2 = \|q_{ij}\|_2 \|m_i - m_j\|_2 \geq |q_{ij}^T(m_i - m_j)| \geq D \quad (15)$$

The resulting constraint $q_{ij}^T(m_i - m_j) \geq D$ is convex and more conservative than the original one (i.e., $\|m_i - m_j\|_2 \geq D$), leading to a convex restriction of the problem and the new feasible set will be a convex subset of the original feasible set. ■

After deriving the convex restriction of constraint (6), we convert the above non-convex problem to an easily solvable problem. Any solution is guaranteed to be feasible for the original non-convex problem and the convexified primal problem is as follows.

Objective: Emplace each UAV v in a proper target location l'_v in 3D space so as to maximize the total amount of data transmitted by UAVs.

$$\max_{l'_v} \sum_{v=1}^{|\mathcal{V}|} \sum_{u=1}^{|\mathcal{U}_{l'_v}|} r_{u,l'_v} \cdot t_{l_v \rightarrow l'_v} \quad (16)$$

$$\text{subject to } P_m t_{m_v \rightarrow m'_v} + P_c t_{h_v \rightarrow h'_v} + (P_h + P_t) t_{l_v \rightarrow l'_v} \leq E_v, \quad \forall v \in \mathcal{V}, l'_v \quad (17)$$

$$q_{vw}^T(m'_v - m'_w) \geq D, \text{where } q_{vw}^T \in \Re^2, \quad \forall v, w \in \mathcal{V}, v < w \quad (18)$$

$$\bar{A} \leq h'_v \leq A, \quad \forall v \in \mathcal{V} \quad (19)$$

$$\sum_{\forall u \in \mathcal{U}_{l'_v}} b_{v,u} \leq B_v, \quad \forall v \in \mathcal{V}, l'_v \quad (20)$$

By conducting the Lagrangian method, we obtain the corresponding Lagrangian function with Lagrange multiplier vectors $\boldsymbol{\lambda} = \{\lambda_v | v \in \mathcal{V}\}$ and $\boldsymbol{\rho} = \{\rho_{vw} | v, w \in \mathcal{V}, v < w\}$, listed below.

$$\begin{aligned}\mathcal{L}(\boldsymbol{l'}, \boldsymbol{\lambda}, \boldsymbol{\rho}) = & \sum_{v=1}^{|\mathcal{V}|} \sum_{u=1}^{|\mathcal{U}_{l'_v}|} r_{u,l'_v} \cdot t_{l_v \rightarrow l'_v} \\ & + \sum_{v=1}^{|\mathcal{V}|} \lambda_v \Big(E_v - P_m t_{m_v \rightarrow m'_v} - P_c t_{h_v \rightarrow h'_v} \\ & \qquad - (P_h + P_t) t_{l_v \rightarrow l'_v} \Big) \\ & + \sum_{v=1}^{|\mathcal{V}|-1} \sum_{w=v+1}^{|\mathcal{V}|} \rho_{vw} \Big(q_{vw}^T(m'_v - m'_w) - D \Big)\end{aligned}$$

Morever, for each pair $(\boldsymbol{\lambda}, \boldsymbol{\rho})$ with $\boldsymbol{\lambda} \succeq \mathbf{0}$ and $\boldsymbol{\rho} \succeq \mathbf{0}$, the Lagrange dual function (10) gives an upper bound on

Authorized licensed use limited to: Korea Univ. Downloaded on February 13,2020 at 05:48:36 UTC from IEEE Xplore. Restrictions apply.

the optimal value $p^\star$ of the convexified primal problem (16), as proved in Lemma 1.

For brevity and ease of reading, the remaining sections will use functional forms to express the objective function and part of constraints:

$$\varphi(\boldsymbol{l'}) = \sum_{v=1}^{|\mathcal{V}|}\sum_{u=1}^{|\mathcal{U}_{l'_v}|} r_{u,l'_v}\cdot t_{l_v\to l'_v}, \quad \boldsymbol{l'} = \{l'_1, l'_2, \cdots, l'_{|\mathcal{V}|}\}$$

$$f_v(l'_v) = E_v - P_m t_{m_v\to m'_v} - P_c t_{h_v\to h'_v} - (P_h+P_t)t_{l_v\to l'_v}, \quad \forall v\in\mathcal{V}$$

$$f_{vw}(m'_v, m'_w) = q_{vw}^T(m'_v - m'_w) - D, \quad \forall v,w\in\mathcal{V}, v<w$$

Lemma 1 (Upper Bound Property): Let $p^\star$ be the primal optimal value of the convexified problem (16). If dual variables $\boldsymbol{\lambda}\succeq\mathbf{0}$ and $\boldsymbol{\rho}\succeq\mathbf{0}$, then $g(\boldsymbol{\lambda},\boldsymbol{\rho})\geq p^\star$.

Proof: Suppose $\widehat{\boldsymbol{l}}$ is primal feasible and $\boldsymbol{\lambda}\succeq\mathbf{0}, \boldsymbol{\rho}\succeq\mathbf{0}$. Then

$$\begin{aligned}\varphi(\widehat{\boldsymbol{l}}) &\leq \varphi(\widehat{\boldsymbol{l}}) + \sum_{v=1}^{|\mathcal{V}|}\lambda_v f_v(\widehat{l_v}) + \sum_{v=1}^{|\mathcal{V}|-1}\sum_{w=v+1}^{|\mathcal{V}|}\rho_{vw} f_{vw}(\widehat{m_v},\widehat{m_w})\\ &= \mathcal{L}(\widehat{\boldsymbol{l}},\boldsymbol{\lambda},\boldsymbol{\rho})\\ &\leq \max_{\boldsymbol{l'}}\ \mathcal{L}(\boldsymbol{l'},\boldsymbol{\lambda},\boldsymbol{\rho})\\ &= g(\boldsymbol{\lambda},\boldsymbol{\rho}) \end{aligned} \tag{21}$$

The first inequality follows because $f_v(\widehat{l_v})$ and $f_{vw}(\widehat{m_v},\widehat{m_w})$ are non-negative for any feasible $\widehat{l_v},\widehat{m_v}$ and $\widehat{m_w}$. The second inequality follows because the feasible point $\widehat{\boldsymbol{l}}$ is constrained by the maximizer selected from all possible feasible points. Since inequality (21) holds for every feasible solution $\widehat{\boldsymbol{l}}$, the upper bound property $g(\boldsymbol{\lambda},\boldsymbol{\rho})\geq p^\star$ follows. ∎

Next, we exploit the Lagrange dual optimization (11) to determine the best upper bound. Although solving the dual problem can provide useful upper bounds for the convexified primal problem (16), the strong duality may not hold if the optimal values of primal and dual problems disagree, yielding a non-zero duality gap. Therefore, we proceed to manifest the strong duality between primal and dual problems and reveal the optimal duality gap.

Definition 1 (Slater's condition): A problem satisfies Slater's condition if it is strictly feasible.

Definition 2 (Strong duality via Slater's condition): If the primal problem is convex and satisfies the weak Slater's condition, then strong duality holds with zero duality gap.

Corollary 1 (Weak Slater's condition): Weak Slater's condition looses strict feasibility when the constraints are all linear equalities and inequalities, and the domain of the objective function is open.

Theorem 2: Strong duality holds for our convexified primal problem (16) and its Lagrange dual problem (11).

Proof: Since the objective function and constraints in the convexified primal problem are all convex, we show strong duality by proving the feasibility on the basis of Definition 1, Definition 2 and Corollary 1. Before starting the proof, we first define several matrices.

$$\mathbb{P} = \begin{bmatrix} P_m & 0\ldots 0\\ P_c & 0\ldots 0\\ (P_h+P_t) & 0\ldots 0\\ 0 & 0\ldots 0\\ \vdots & \vdots\ddots\vdots\\ 0 & 0\ldots 0\end{bmatrix}^T \quad \mathbb{T} = \begin{bmatrix} t_{m_1\to m'_1} & \ldots & t_{m_{|\mathcal{V}|}\to m'_{|\mathcal{V}|}}\\ t_{h_1\to h'_1} & \ldots & t_{h_{|\mathcal{V}|}\to h'_{|\mathcal{V}|}}\\ t_{l_1\to l'_1} & \ldots & t_{l_{|\mathcal{V}|}\to l'_{|\mathcal{V}|}}\\ 0 & \ldots & 0\\ \vdots & \ddots & \vdots\\ 0 & \ldots & 0\end{bmatrix}$$

$$\mathbb{E} = \begin{bmatrix} E_1 & E_2 & \ldots & E_{|\mathcal{V}|}\\ 0 & 0 & \ldots & 0\\ \vdots & \vdots & \ddots & \vdots\\ 0 & 0 & \ldots & 0\end{bmatrix} \quad \mathbb{Q} = \begin{bmatrix} 0 & q_{12}^T & q_{13}^T & \cdots & q_{1|\mathcal{V}|}^T\\ 0 & 0 & q_{23}^T & \cdots & q_{2|\mathcal{V}|}^T\\ \vdots & \vdots & \vdots & \ddots & \vdots\\ 0 & 0 & 0 & \ldots & q_{|\mathcal{V}|-1|\mathcal{V}|}^T\\ 0 & 0 & 0 & \ldots & 0\end{bmatrix}$$

$$\mathbb{M} = \begin{bmatrix} 0 & m'_{12} & m'_{13} & \ldots & m'_{1|\mathcal{V}|}\\ 0 & 0 & m'_{23} & \ldots & m'_{2|\mathcal{V}|}\\ \vdots & \vdots & \vdots & \ddots & \vdots\\ 0 & 0 & 0 & \ldots & m'_{|\mathcal{V}|-1|\mathcal{V}|}\\ 0 & 0 & 0 & \ldots & 0\end{bmatrix} \quad \mathbb{H} = \begin{bmatrix} h'_1\\ h'_2\\ \vdots\\ h'_{|\mathcal{V}|}\end{bmatrix} \quad \mathbb{B} = \begin{bmatrix} B_1\\ B_2\\ \vdots\\ B_{|\mathcal{V}|}\end{bmatrix}$$

$$\mathbb{C} = \begin{bmatrix} b_{1,1} & b_{2,1} & b_{3,1} & \ldots & b_{|\mathcal{U}|,1}\\ b_{1,2} & b_{2,2} & b_{3,2} & \ldots & b_{|\mathcal{U}|,2}\\ \vdots & \vdots & \vdots & \ddots & \vdots\\ b_{1,|\mathcal{V}|} & b_{2,|\mathcal{V}|} & b_{3,|\mathcal{V}|} & \ldots & b_{|\mathcal{U}|,|\mathcal{V}|}\end{bmatrix} \mathbb{J} = \begin{bmatrix}1\\1\\\vdots\\1\end{bmatrix}_{|\mathcal{U}|\times 1} \quad \mathbb{I} = \begin{bmatrix}1\\1\\\vdots\\1\end{bmatrix}_{|\mathcal{V}|\times 1}$$

where $\mathbb{T},\mathbb{P},\mathbb{E},\mathbb{Q}$ and $\mathbb{M}$ are all $|\mathcal{V}|$ by $|\mathcal{V}|$ matrices. $\mathbb{C}$ is a $|\mathcal{V}|$ by $|\mathcal{U}|$ matrix. $m'_{ij} = m'_i - m'_j = [x'_i - x'_j \quad y'_i - y'_j]^T$ and $q_{ij} = \frac{m'_{ij}}{\|m'_{ij}\|_2}$. Moreover, $\mathbb{I}$ and $\mathbb{J}$ are $|\mathcal{V}|$ by 1 and $|\mathcal{U}|$ by 1 identity column vectors, respectively. Constraints (17)-(20) can be rewritten as

$$\begin{aligned}\mathbb{P}\mathbb{T} &\preceq \mathbb{E}\\ tr(\mathbb{Q}\mathbb{M}^T) &\geq \frac{|\mathcal{V}|(|\mathcal{V}|-1)}{2}D\\ \bar{A}\mathbb{I} &\preceq \mathbb{H} \preceq A\mathbb{I}\\ \mathbb{C}\mathbb{J} &\preceq \mathbb{B}\end{aligned}$$

where $tr(\cdot)$ stands for the trace operation. Then, we can find feasible solutions $\widehat{\mathbb{M}}$ and $\widehat{\mathbb{C}}$ under a feasible solution $\widehat{\mathbb{H}}$, leading to a feasible solution $\widehat{\mathbb{T}}$:

$$\begin{aligned}\mathbb{P}\widehat{\mathbb{T}} \preceq \mathbb{E} &\Leftrightarrow \mathbb{P}\widehat{\mathbb{T}} + \Theta = \mathbb{E}\\ &\Leftrightarrow \mathbb{P}\widehat{\mathbb{T}} = \mathbb{E} - \Theta\\ &\Leftrightarrow \widehat{\mathbb{T}} = \mathbb{P}^{-1}(\mathbb{E}-\Theta)\end{aligned}$$

There must exist a matrix Θ such that $\widehat{\mathbb{T}}$ is feasible. Hence, a feasible solution $(\widehat{\mathbb{T}},\widehat{\mathbb{M}},\widehat{\mathbb{H}},\widehat{\mathbb{C}})$ is discovered for the convexified primal problem, which satisfies the constraints:

$$\begin{aligned}\mathbb{P}\widehat{\mathbb{T}} &\preceq \mathbb{E}\\ tr(\mathbb{Q}\widehat{\mathbb{M}}^T) &\geq \frac{|\mathcal{V}|(|\mathcal{V}|-1)}{2}D\\ \bar{A}\mathbb{I} &\preceq \widehat{\mathbb{H}} \preceq A\mathbb{I}\\ \widehat{\mathbb{C}}\mathbb{J} &\preceq \mathbb{B}\end{aligned}$$

As a result, the proof of strong duality is complete from both aspects of convexity and feasibility. ∎

Authorized licensed use limited to: Korea Univ. Downloaded on February 13,2020 at 05:48:36 UTC from IEEE Xplore. Restrictions apply.

Here, Slater's condition not only implies that strong duality holds but also that the dual optimum is obtained. To demonstrate the relationship between primal and dual optimal solutions, we further employ Karush-Kuhn-Tucker (KKT) optimality conditions.

Theorem 3: If a convex optimization problem with differentiable objective and constraint functions fulfills Slater's condition, then the KKT conditions provide necessary and sufficient conditions for optimality: $\boldsymbol{l}^\star$ is primal optimal if and only if there are $(\boldsymbol{\lambda}^\star, \boldsymbol{\rho}^\star)$ that, together with $\boldsymbol{l}^\star$, satisfy the KKT conditions.

Proof: The KKT conditions typically include:

1) Primal feasibility.

$$\begin{aligned} f_v(l_v^\star) &\geq 0, \quad \forall v \in \mathcal{V} \\ f_{vw}(m_v^\star, m_w^\star) &\geq 0, \quad \forall v, w \in \mathcal{V}, v < w \\ \bar{A} \leq h_v^\star &\leq A, \quad \forall v \in \mathcal{V} \\ \sum_{\forall u \in \mathcal{U}_{l_v^\star}} b_{v,u}^\star &\leq B_v, \quad \forall v \in \mathcal{V} \end{aligned}$$

2) Dual feasibility.

$$\boldsymbol{\lambda}^\star \succeq \mathbf{0}, \quad \boldsymbol{\rho}^\star \succeq \mathbf{0}$$

3) Complementary slackness.

$$\begin{aligned} \lambda_v^\star \, f_v(l_v^\star) &= 0, \quad \forall v \in \mathcal{V} \\ \rho_{vw}^\star \, f_{vw}(m_v^\star, m_w^\star) &= 0, \quad \forall v, w \in \mathcal{V}, v < w \end{aligned}$$

4) $\boldsymbol{l}^\star$ maximizes $\mathcal{L}(\boldsymbol{l'}, \boldsymbol{\lambda}^\star, \boldsymbol{\rho}^\star)$ over $\boldsymbol{l'}$, so its gradient with respect to $\boldsymbol{l'}$ vanishes at $\boldsymbol{l'} = \boldsymbol{l}^\star$.

$$\begin{aligned} \nabla_{\boldsymbol{l'}} \mathcal{L}(\boldsymbol{l'}, \boldsymbol{\lambda}^\star, \boldsymbol{\rho}^\star) &= \nabla \varphi(\boldsymbol{l}^\star) + \sum_{v=1}^{|\mathcal{V}|} \lambda_v^\star \nabla f_v(l_v^\star) \\ &\quad + \sum_{v=1}^{|\mathcal{V}|-1} \sum_{w=v+1}^{|\mathcal{V}|} \rho_{vw}^\star \nabla f_{vw}(m_v^\star, m_w^\star) \\ &= \mathbf{0} \end{aligned}$$

The first condition shows that $\boldsymbol{l}^\star$ is primal feasible. Because $\boldsymbol{\lambda}^\star \succeq \mathbf{0}$ and $\boldsymbol{\rho}^\star \succeq \mathbf{0}$, the Lagrangian $\mathcal{L}(\boldsymbol{l'}, \boldsymbol{\lambda}^\star, \boldsymbol{\rho}^\star)$ is convex in $\boldsymbol{l'}$. The complementary slackness property specified in Condition 3 makes $\lambda_v^\star$ and $\rho_{vw}^\star$ zero unless the corresponding constraint is active at the optimum, with the detailed proof given in Lemma 2. Condition 4 states that $\boldsymbol{l}^\star$ is the maximizer of $\mathcal{L}(\boldsymbol{l'}, \boldsymbol{\lambda}^\star, \boldsymbol{\rho}^\star)$. In summary,

$$\begin{aligned} g(\boldsymbol{\lambda}^\star, \boldsymbol{\rho}^\star) &= \mathcal{L}(\boldsymbol{l}^\star, \boldsymbol{\lambda}^\star, \boldsymbol{\rho}^\star) \\ &= \varphi(\boldsymbol{l}^\star) + \sum_{v=1}^{|\mathcal{V}|} \lambda_v^\star \, f_v(l_v^\star) \\ &\quad + \sum_{v=1}^{|\mathcal{V}|-1} \sum_{w=v+1}^{|\mathcal{V}|} \rho_{vw}^\star \, f_{vw}(m_v^\star, m_w^\star) \\ &= \varphi(\boldsymbol{l}^\star) \end{aligned}$$

The last line holds because of the complementary slackness property. Hence, we conclude that $\boldsymbol{l}^\star$ and $(\boldsymbol{\lambda}^\star, \boldsymbol{\rho}^\star)$ are respectively the primal and dual optimal. ∎

Lemma 2: Suppose strong duality holds. $\boldsymbol{l}^\star$ is primal optimal if there exists a dual feasible $(\boldsymbol{\lambda}^\star, \boldsymbol{\rho}^\star)$ such that the complementary slackness conditions hold.

Proof: According to strong duality, we have

$$\begin{aligned} \varphi(\boldsymbol{l}^\star) &= g(\boldsymbol{\lambda}^\star, \boldsymbol{\rho}^\star) \\ &= \max_{\boldsymbol{l'}} \Bigg\{ \varphi(\boldsymbol{l'}) + \sum_{v=1}^{|\mathcal{V}|} \lambda_v^\star f_v(l_v') \\ &\qquad + \sum_{v=1}^{|\mathcal{V}|-1} \sum_{w=v+1}^{|\mathcal{V}|} \rho_{vw}^\star f_{vw}(m_v', m_w') \Bigg\} \\ &\geq \varphi(\boldsymbol{l}^\star) + \sum_{v=1}^{|\mathcal{V}|} \lambda_v^\star f_v(l_v^\star) + \sum_{v=1}^{|\mathcal{V}|-1} \sum_{w=v+1}^{|\mathcal{V}|} \rho_{vw}^\star f_{vw}(m_v^\star, m_w^\star) \\ &\geq \varphi(\boldsymbol{l}^\star) \end{aligned}$$

The first line exhibits zero duality gap by strong duality and the second equality follows from the definition of the dual function. The third line follows because the maximum of the Lagrangian over $\boldsymbol{l'}$ is larger than or equal to its value at $\boldsymbol{l'} = \boldsymbol{l}^\star$. The last line follows from $\lambda_v^\star \geq 0, f_v(l_v^\star) \geq 0, \forall v \in \mathcal{V}$ and $\rho_{vw}^\star \geq 0, f_{vw}(m_v^\star, m_w^\star) \geq 0, \forall v, w \in \mathcal{V}, v < w$. Thus, the two inequalities in this chain hold with equality.

We conclude that $\boldsymbol{l}^\star$ is the maximizer of $\mathcal{L}(\boldsymbol{l'}, \boldsymbol{\lambda}^\star, \boldsymbol{\rho}^\star)$:

$$\varphi(\boldsymbol{l}^\star) = \varphi(\boldsymbol{l}^\star) + \sum_{v=1}^{|\mathcal{V}|} \lambda_v^\star f_v(l_v^\star) + \sum_{v=1}^{|\mathcal{V}|-1} \sum_{w=v+1}^{|\mathcal{V}|} \rho_{vw}^\star f_{vw}(m_v^\star, m_w^\star)$$

Therefore,

$$\begin{aligned} \lambda_v^\star f_v(l_v^\star) &= 0, \quad \forall v \in \mathcal{V} \\ \rho_{vw}^\star f_{vw}(m_v^\star, m_w^\star) &= 0, \quad \forall v, w \in \mathcal{V}, v < w \end{aligned}$$

∎

We then perform the proposed *EAUD* algorithm to locate UAVs at proper locations, with the following Lagrange multiplier vectors:

$$\begin{aligned} &\lambda_v(k+1) \\ &= \left[\lambda_v(k) - \beta(k) \frac{\partial g(\boldsymbol{\lambda}(k), \boldsymbol{\rho}(k))}{\partial \lambda_v(k)} \right]^+ \\ &= \Bigg[\lambda_v(k) - \beta(k) \Big(E_v(k) - P_m(k) t_{m_v \to m_v'}(k) \\ &\qquad - P_c(k) t_{h_v \to h_v'}(k) - \Big(P_h(k) + P_t(k) \Big) t_{l_v \to l_v'}(k) \Big) \Bigg]^+, \\ &\qquad\qquad \forall v \in \mathcal{V} \end{aligned} \tag{22}$$

$$\begin{aligned} &\rho_{vw}(k+1) \\ &= \left[\rho_{vw}(k) - \beta(k) \frac{\partial g(\boldsymbol{\lambda}(k), \boldsymbol{\rho}(k))}{\partial \rho_{vw}(k)} \right]^+ \\ &= \left[\rho_{vw}(k) - \beta(k) \Big(q_{vw}^T(k) \Big(m_v'(k) - m_w'(k) \Big) - D(k) \Big) \right]^+, \\ &\qquad\qquad \forall v, w \in \mathcal{V}, v < w \end{aligned} \tag{23}$$

where $[\alpha]^+ = \max\{0, \alpha\}$ and $\beta(k) > 0$ indicates the step size at the k-th iteration.

Authorized licensed use limited to: Korea Univ. Downloaded on February 13,2020 at 05:48:36 UTC from IEEE Xplore. Restrictions apply.

V. Implementation Remarks

In this section, we discuss some implementation issues for operating the proposed *EAUD* algorithm in next-generation cellular networks.

- *Input data collection*: The implementation environment consists of a land-based GCS plus a swarm of UAVs. The GCS is responsible for controlling and managing multiple UAVs and each UAV powered by batteries is equipped with a base station for data delivery. At predefined time intervals, the GCS performs the proposed 3D deployment algorithm at the start of each flight plan with the necessary input information. The inputs for the *EAUD* algorithm can be roughly classified into two categories: channel condition information and user location information. Referring to the existing components of base stations, the channel condition information can be easily obtained. As to the user location information, there are two prevalent methods: one is based on historical location traces [38], and the other is based on the statistical prediction [39]. For the former one, fingerprint-based and geometry-based techniques utilize radio-frequency signals from stationary sources and the knowledge of the actual user positions to identify the spatio-temporal localization of users, respectively. For the latter one, plenty of schemes based on user mobility patterns are available to profile the spatial distribution of users, such as the density estimation model and the feature fusion model.
- *Deployment issues*: In a real-world environment, many efforts are underway to integrate UAV operations safely and routinely into civil airspace. For safety reasons, the UAV deployment is currently confined to special-use airspace with air traffic control permission. Regulatory authorities such as FAA and Transport Canada formulate rules to govern the manipulation of UAVs in various aspects: maximum flight altitude, allowable flight time in a day, maximum flying speed, maximum payload weight, weather condition and visibility, and so on. Our proposed algorithm can be directly applied without any modification as long as the settings of the above-mentioned parameters conform to the regulations.

VI. Performance Evaluation

In this section, we evaluate our proposed approach, *Energy-Aware 3D UAV Deployment (EAUD)*, by conducting extensive simulations and then give insights into the simulation results.

A. Simulation Setups

We build a MATLAB simulator to evaluate the performance of our *EAUD* scheme in an urban outdoor free-space environment with the following settings. The system bandwidth is 15 MHz. There are between 1 and 15 UAVs inside a simulation area of size 500 $\times$ 500 m^2. All of the UAVs are homogeneous and initially located on the ground at the center of the simulation field. Under the regulations of FAA [33], each UAV navigates between altitudes of 16.46 m and 33.22 m in the airspace and the corresponding ground coverage radius falls within the extent of 50 m to 100 m [11]. The available energy budget for a UAV ranges from 200 kJ to 300 kJ and the average power consumed by movement, hovering and climbing are measured as 240 W, 210 W and 85 W, respectively [40], [41]. Based on 3GPP's heterogeneous system setting [42], the minimum inter-UAV distance is set as 40 m.

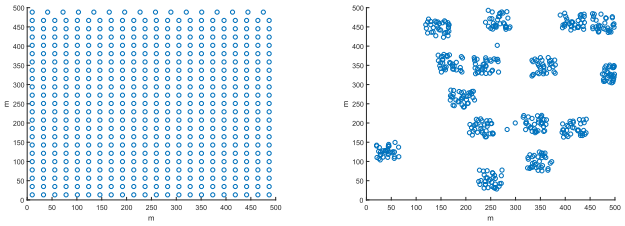

(a) Uniform user distribution. (b) Non-uniform user distribution.

Fig. 2. Different user distribution scenarios.

TABLE II
Parameter Settings

Parameter	Value
The simulation area	500 $\times$ 500 m^2
The number of users in the system	500
The number of UAVs	1 ~ 15
The radius of a UAV [11]	50 ~ 100 m
The minimum altitude of a UAV	16.46 m
The maximum altitude of a UAV	33.22 m
Energy budget of a UAV	200 ~ 300 kJ
The average power consumed by a UAV during movement [40]	240 W
The average power consumed by a UAV when hovering [40]	210 W
The average power consumed by a UAV in climbing [41]	85 W
The minimum inter-UAV distance [42]	40 m
System bandwidth	15 MHz

In our cellular system, 500 users are deployed using two distribution scenarios: one is uniform and the other is non-uniform, as shown in Fig. 2. For the uniform distribution case such as at parking lots, users are arranged uniformly in a grid manner. For the non-uniform distribution case, we adopt the clustered UE (user equipment) placement model specified in 3GPP [42] to distribute users in accordance with the observation that following the clustering effect, users often gather in certain "hotzones" in urban areas, such as stadiums and plazas [43]. The following represents the model.

$$N_h = \left\lfloor p \cdot \frac{|\mathcal{U}|}{|\mathcal{V}|} \right\rfloor, \tag{24}$$

where N_h denotes the number of users distributed in a hotzone area and p is the proportion of all hotzone users to the total number of users in the network. $|\mathcal{U}|$ and $|\mathcal{V}|$ are respectively the total number of users and UAVs. After finishing the allocation of hotzone users, the remaining $(|\mathcal{U}| - N_h \times |\mathcal{V}|)$ users are randomly dispersed within the coverage of macrocells. Table II lists the parameter settings.

B. Comparison Approaches

Unlike only focusing on the transmit power as previous literature, our proposed *EAUD* deployment pays attention to the power consumption of in-flight activities as well. To justify

Authorized licensed use limited to: Korea Univ. Downloaded on February 13,2020 at 05:48:36 UTC from IEEE Xplore. Restrictions apply.

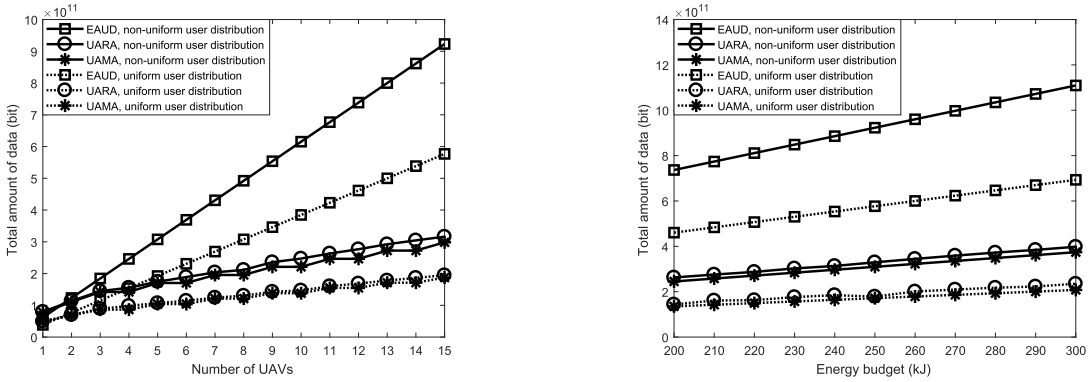

(a) Under the available energy budget of 250 kJ per UAV. (b) Under the scenario of 15 UAVs.

Fig. 3. The separate impacts of the number of UAVs and the available energy budget on the total amount of data transmitted by UAVs.

the important observation about the significant difference in energy expenditure between communications (a few watts) and maneuvering operations (hundreds of watts) [40], [41], we are attentive to the design of comparison approaches for highlighting the trade-off effects. Intuitively, either high-density places or low-altitude flights will boost the total amount of data. Consequently, we compare our proposed *EAUD* algorithm against the following two approaches in terms of five performance metrics: total amount of data transmitted by UAVs, average flight time per UAV, average service time per UAV, service power ratio and energy efficiency.

1) User-Aware Approach With a Random Altitude Assignment: This approach, termed as *UARA*, deploys UAVs in a manner that is consistent with the goal of enhancing both network coverage and capacity according to the user distribution. That is, UAVs will leverage their mobility abilities to fly to the places with high user density. In this case, each UAV randomly selects an altitude from the specific allowed interval and remains afloat in the air until almost running out of energy.

2) User-Aware Approach With a Minimum Altitude Assignment: The core concept of this approach, expressed as *UAMA*, is similar to that of *UARA*. Accordingly, in this scheme, UAVs are prone to fly over densely populated areas so as to provide services for as many users as possible. Instead of picking a random altitude at will, each UAV always flies at the minimum altitude level.

C. Simulation Results

This section presents in-depth discussions on the simulation results with regard to diverse performance metrics.

1) Total Amount of Data Transmitted by UAVs: Fig. 3 demonstrates how the number of UAVs and the available energy budget affect the total amount of network data. It is quite obvious that more users can be serviced as more UAVs join in the network, resulting in a higher total amount of data transmitted by UAVs. As Fig. 3(a) shows, compared to both *UARA* and *UAMA*, our proposed *EAUD* scheme can achieve remarkable improvement in the total amount of data. The main reason lies in the ways to select target locations. Each UAV in our proposed scheme will discover its target location by jointly considering the travel time spent before getting to its destination, the number of covered users relative to different flight altitudes and the energy expenses on diverse maneuvering operations. However, a UAV in *UARA* and *UAMA* schemes may take a long travel time to arrive at a remote site with high user density, thus sacrificing the service time, the battery life and further the total amount of data. From the simulation results, we observe that *UARA* displays a little superior performance than *UAMA*. Although users being served in *UAMA* scheme can enjoy higher data rates than those in *UARA* scheme, the large number of served users derived from possible large coverage areas enables *UARA* scheme to contribute more aggregate data rates to the total amount of data. In addition, we also observe the impacts of different distribution scenarios on the total amount of data. Since the uniform user distribution exhibits a regular and sparse pattern, each UAV flying at the same altitude as the non-uniform case can only cover relatively few users. Therefore, the scenario of non-uniform user distribution has better performance than the uniform one no matter what scheme is applied.

Fig. 3(b) shows the impacts of the available energy budget on the total amount of data transmitted by UAVs under the scenario of 15 UAVs. Because a larger energy budget implies a longer lifetime in the network, the total amount of data transmitted by UAVs increases with the available energy budget. Furthermore, abundant amounts of available energy not only allow for farther flights but also prolong service time potentially. As a result, UAVs can fly to the places at favorable altitudes either with more served users or with higher data rates to produce more amount of data. Simulation results show that *EAUD* outperforms both *UARA* and *UAMA* schemes because of its ability to tackle the spatial and temporal trade-off issue among flight altitude, travel time and battery life properly. We can also observe the trade-off issue from Fig. 3 and Fig. 7. On the other hand, although the poor signal strengths under *UARA* damage the total amount of data transmitted by UAVs, the probable increase in the number of served users compensates for the loss, yielding a marginal improvement in comparison with *UAMA* scheme.

- *Tolerance Threshold Determination:* Fig. 4 exhibits the impacts of the number of UAVs on the total amount

Authorized licensed use limited to: Korea Univ. Downloaded on February 13,2020 at 05:48:36 UTC from IEEE Xplore. Restrictions apply.

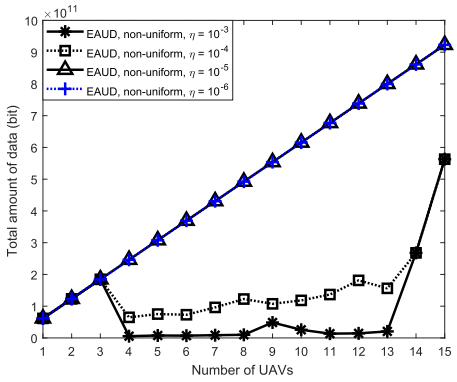

(a) Non-uniform user distribution.

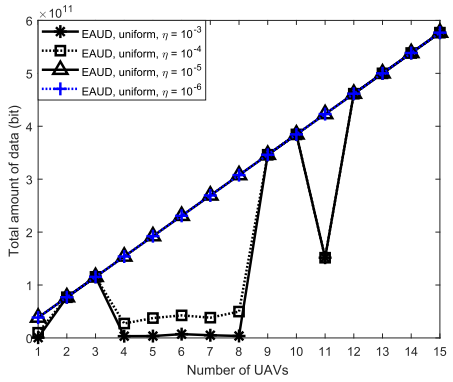

(b) Uniform user distribution.

Fig. 4. The impacts of the number of UAVs on the total amount of data transmitted by UAV under the available energy budget of 250 kJ per UAV.

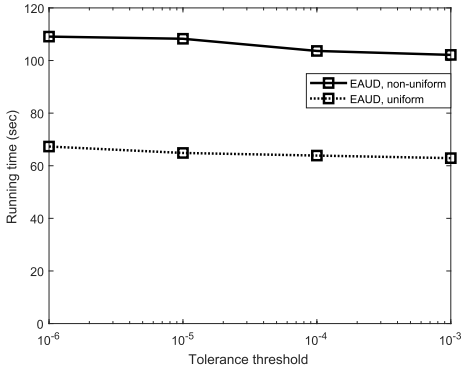

Fig. 5. The running time required by *EAUD* algorithm under distinct tolerance thresholds.

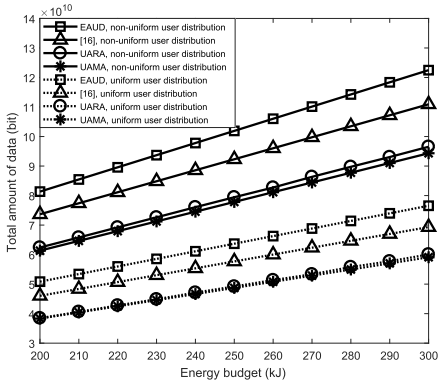

Fig. 6. The impacts of the available energy budget on the total amount of data transmitted by UAVs.

of data transmitted by UAVs under the *EAUD* scheme. Recall that the tolerance threshold η is used to judge whether an optimal solution is convergent or not, i.e., the difference in optimal solutions for each UAV between two consecutive iterations should be smaller than η. As expected, the smaller the tolerance threshold η, the more stable the performance of the total amount of data. When employing a large value of η, a feasible solution is relatively easily found to meet the constraint, but may be trapped into a local optimum. Therefore, high uncertainty and great instability in the total amount of data occur in both non-uniform and uniform user distributions. From the simulation results, the performance of the total amount of data tends to increase steadily as η is below 10^{-5}. As Fig. 5 shows, although a small η takes slightly more time to find out optimal solutions than a large η, the overall running time for the four different thresholds is within two minutes which is applicable for the 3D UAV deployment. Based on this observation, this paper adopts $\eta = 10^{-6}$ to run all the simulations for better and stable performance.

- *Comparison Results for A Single UAV Case:* Here, we consider another comparison approach proposed in [16]: a study of the 3D placement problem of a single UAV that aims at maximizing the number of covered users. Similar to *UARA* and *UAMA* schemes, the main notion of the approach proposed in [16] is to locate the UAV at a place with high user density. Nevertheless, the flight altitude in [16] is determined by the formulated optimization problem. Due to the proper selection of the flight altitude in [16], a higher total amount of data can be achieved compared to both *UARA* and *UAMA*, as shown in Table III and Fig. 6. On the other hand, the scheme proposed in 16] exhibits a worse performance than our *EAUD* scheme without the consideration of the limited energy budget.

TABLE III

TOTAL AMOUNT OF DATA FOR EACH ALGORITHM WHEN DEPLOYING ONLY A SINGLE UAV (Gbit)

Algorithm	EAUD	[16]	UARA	UAMA
Non-uniform user distribution	101.91	88.3	85.49	84.05
Uniform user distribution	63.69	55.18	53.35	52.96

2) Average Flight Time Per UAV: Fig. 7 portrays the influence of the number of UAVs and the available energy budget on the average flight time per UAV. Here, the flight time of a UAV is composed of its horizontal movement and vertical climbing time lapses. In order to avoid the co-tier interference, any new addition of UAVs will trigger a rearrangement of locations for greater profit gains. Since the design concepts

Authorized licensed use limited to: Korea Univ. Downloaded on February 13,2020 at 05:48:36 UTC from IEEE Xplore. Restrictions apply.

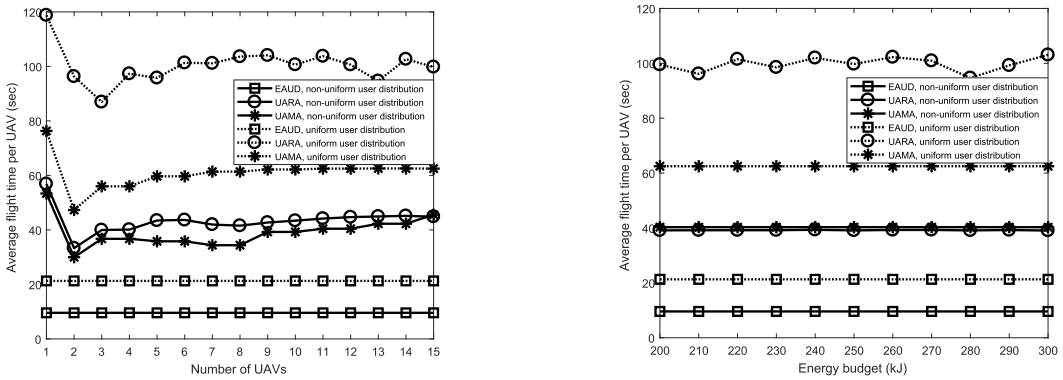

(a) Under the available energy budget of 250 kJ per UAV. (b) Under the scenario of 15 UAVs.

Fig. 7. The separate impacts of the number of UAVs and the available energy budget on the average flight time per UAV.

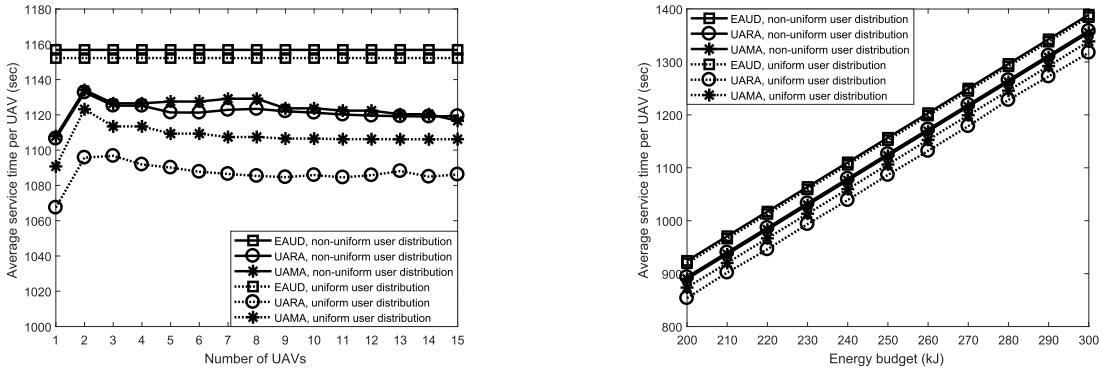

(a) Under the available energy budget of 250 kJ per UAV. (b) Under the scenario of 15 UAVs.

Fig. 8. The separate impacts of the number of UAVs and the available energy budget on the average service time per UAV.

of both *UARA* and *UAMA* strategies are locating the high density areas in the network, the actual UAV deployment highly depends on the user distribution. However, our *EAUD* scheme will fully utilize all available UAVs to raise the system performance without the necessity of locating at places with high crowd density. Consequently, UAVs in *EAUD* spend the least amounts of time in transit to their ideal target locations compared with those in *UARA* and *UAMA* schemes, as shown in Fig. 7(a). On the other hand, we witness the instability of flight time expenses under both *UARA* and *UAMA* schemes. The performance gap is especially apparent for the scenario of uniform user distribution as a result of sparse user arrangements. Due to the randomness of flight altitudes, UAVs in *UARA* therefore take much longer time to travel to suitable and interference-free positions than those in *UAMA*. In addition, in contrast to the fluctuations presented in *UARA* and *UAMA*, our proposed *EAUD* scheme is prone to realize the fairness of the average flight time among UAVs in terms of different number of UAVs. As the flight plan is mainly determined by the network topology, for a given number of UAVs, there is no significant impact of the available energy budget on the average flight time per UAV, as shown in Fig. 7(b).

3) Average Service Time Per UAV: Fig. 8 shows the influence of the number of UAVs and the available energy budget on the average service time per UAV. The service time of a UAV here refers to the period of time a UAV supplies services to users when hovering over its target location. As expected, given a fixed energy budget, the shorter the flight time, the longer the service time. Therefore, all curves in Fig. 8(a) appear in reverse order of the ones in Fig. 7(a). As Fig. 8(b) shows, the average service time per UAV for all the three algorithms increases with the available energy budget. The reason is that more energy supply will potentially elongate the lifetime of UAVs in the air under the same network topology. Besides, more energy not only furnishes more options for proper emplacement but also enables UAVs to make long-distance travels for good destinations. Generally speaking, our proposed *EAUD* approach ensures that UAVs always fly to appropriate locations in a time-saving manner irrespective of distinct user distribution scenarios and the resulting longer service provisioning time facilitates a large increase in the total amount of data.

4) Service Power Ratio: Fig. 9 depicts the impacts of the number of UAVs and the available energy budget on the service power ratio. When reaching the target location, a UAV hovers there and then commences to provide services to users. Service power ratio is hence measured as the fraction of the energy expenditure arising from hovering and data transmission over the total energy consumption. Since hovering operation is the dominant energy consumer among all maneuvering and transmission operations during

Authorized licensed use limited to: Korea Univ. Downloaded on February 13,2020 at 05:48:36 UTC from IEEE Xplore. Restrictions apply.

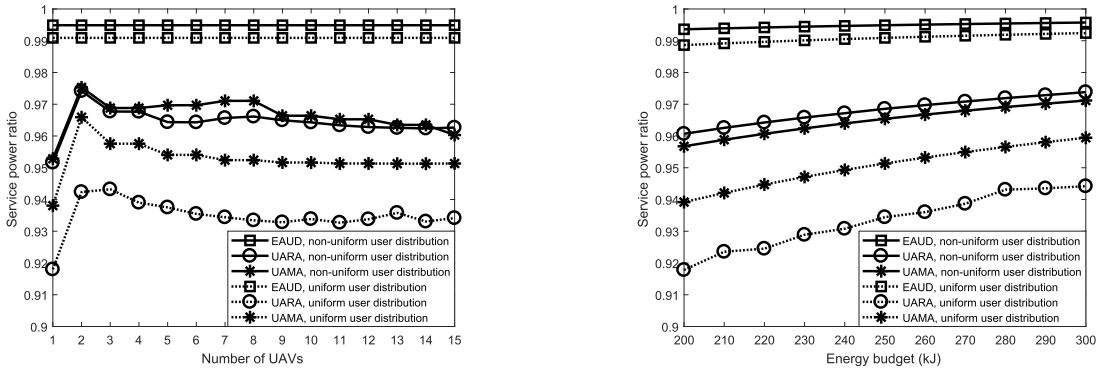

(a) Under the available energy budget of 250 kJ per UAV. (b) Under the scenario of 15 UAVs.

Fig. 9. The individual impacts of the number of UAVs and the available energy budget on the service power ratio.

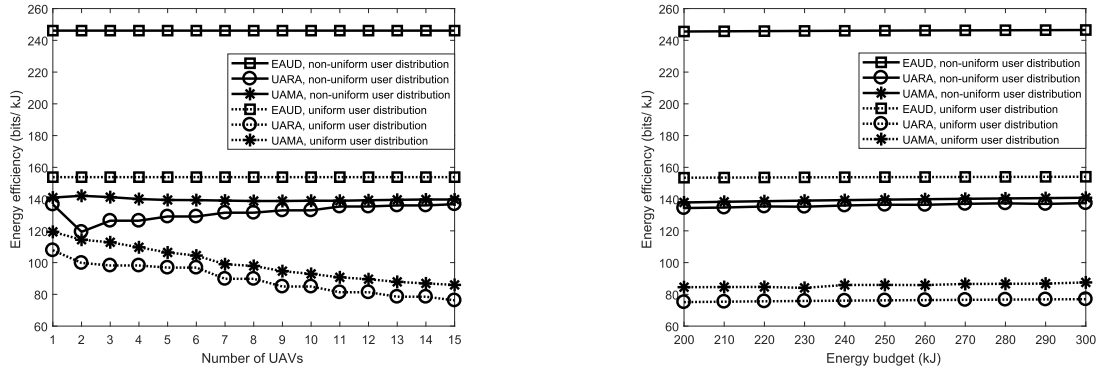

(a) Under the available energy budget of 250 kJ per UAV. (b) Under the scenario of 15 UAVs.

Fig. 10. The individual impacts of the number of UAVs and the available energy budget on the energy efficiency.

the service periods, the service power ratio will primarily vary with the length of the service time. In consequence, the curve trends in Fig. 9(a) are consistent with the average service time per UAV shown in Fig. 8(a). On the other hand, as mentioned previously, the lifespan of a UAV relates directly to its available energy budget, so a larger energy budget allows for a longer service provisioning time at the cost of depleting more energy, as shown in Fig. 9(b). On the whole, the greater the increase in service time, the higher rise in energy burdens. Even with such negative effects, a pretty good improvement in the total amount of data of all users can be achieved by properly maneuvering UAVs.

5) Energy Efficiency: Fig. 10 investigates the impacts of the number of UAVs and the available energy budget on the energy efficiency. We use the energy efficiency, the unit of quantity of bits per kilojoule, as an indicator to unveil the effectiveness of the UAV deployment. Simulation results show that UAVs in our proposed *EAUD* scheme can fully exert their effects under both non-uniform and uniform user distribution scenarios. As Fig. 10(a) shows, *EAUD* outperforms the other two schemes because the space-time trade-off issue among flight altitude, travel distance and battery life is well handled. In the meantime, since *UAMA* always deploys UAVs at the minimum altitude level, the higher data rate and the lower energy overhead make *UAMA* better than *UARA*. Furthermore, a steady and slight growth in energy efficiency continues with the rise in the available energy budget on account of long network lifetime, as shown in Fig. 10(b). Nevertheless, a too sparse user distribution will deteriorate the overall system performance, as illustrated in the uniform distribution case.

VII. Conclusion

This paper studies the 3D deployment problem by using a fleet of UAVs equipped with small cells in next generation cellular networks. Based on the observation that maneuvering operations play an important role in the entire power expenses, our objective is to maximize the total amount of data transmitted by UAVs subject to the flight altitude, the travel time and the energy expenditure of UAVs. We formulate our target problem as a non-convex non-linear optimization problem, followed by a proposal to resolve it by exploiting Lagrangian dual relaxation, interior-point and subgradient projection methods. Then, we illustrate the proof of the optimality of a special case after completing the transformation from the general non-convex non-linear problem into a convexified linear one. Finally, we construct several simulations to demonstrate the efficacy of our proposed algorithm in terms of diverse performance metrics.

References

[1] *Global Mobile Data Traffic Forecast Update*, Cisco, San Jose, CA, USA, Mar. 2017. [Online]. Available: https://www.cisco.com/c/en/us/solutions/collateral/service-provider/visual-n% etworking-index-vni/mobile-white-paper-c11-520862.html

Authorized licensed use limited to: Korea Univ. Downloaded on February 13,2020 at 05:48:36 UTC from IEEE Xplore. Restrictions apply.

[2] J. G. Andrews *et al.*, "What will 5G be?" *IEEE J. Sel. Areas Commun.*, vol. 32, no. 6, pp. 1065–1082, Jun. 2014.

[3] S.-F. Chou, T.-C. Chiu, Y.-J. Yu, and A.-C. Pang, "Mobile small cell deployment for next generation cellular networks," in *Proc. GLOBECOM*, Dec. 2014, pp. 4852–4857.

[4] S.-F. Chou, Y.-J. Yu, and A.-C. Pang, "Mobile small cell deployment for service time maximization over next-generation cellular networks," *IEEE Trans. Veh. Technol.*, vol. 66, no. 6, pp. 5398–5408, Jun. 2017.

[5] Y. Zeng, R. Zhang, and T. J. Lim, "Wireless communications with unmanned aerial vehicles: Opportunities and challenges," *IEEE Commun. Mag.*, vol. 54, no. 5, pp. 36–42, May 2016.

[6] Google. (2018). *Project Loon*. [Online]. Available: https://www.google.com/loon/

[7] ABSOLUTE. (Oct. 2012). *Next Generation Public Safety Systems*. [Online]. Available: http://www.absolute-project.eu/

[8] J. Chen *et al.*, "Long-range and broadband aerial communication using directional antennas (ACDA): Design and implementation," *IEEE Trans. Veh. Technol.*, vol. 66, no. 12, pp. 10793–10805, Dec. 2017.

[9] D. H. Choi, S. H. Kim, and D. K. Sung, "Energy-efficient maneuvering and communication of a single UAV-based relay," *IEEE Trans. Aerosp. Electron. Syst.*, vol. 50, no. 3, pp. 2320–2327, Jul. 2014.

[10] *Feasibility Study on New Services and Markets Technology Enablers for Critical Communications*, document TR 22.862, Version 14.1.0, 3GPP, Sep. 2016.

[11] A. Al-Hourani, S. Kandeepan, and S. Lardner, "Optimal LAP altitude for maximum coverage," *IEEE Wireless Commun. Lett.*, vol. 3, no. 6, pp. 569–572, Dec. 2014.

[12] M. Mozaffari, W. Saad, M. Bennis, and M. Debbah, "Drone small cells in the clouds: Design, deployment and performance analysis," in *Proc. GLOBECOM*, Dec. 2015, pp. 1–6.

[13] N. Goddemeier, S. Rohde, J. Pojda, and C. Wietfeld, "Evaluation of potential fields mobility strategies for aerial network provisioning," in *Proc. IEEE Globecom Workshops*, Dec. 2011, pp. 1291–1296.

[14] J. Lyu, Y. Zeng, R. Zhang, and T. J. Lim, "Placement optimization of UAV-mounted mobile base stations," *IEEE Commun. Lett.*, vol. 21, no. 3, pp. 604–607, Mar. 2017.

[15] A. Merwaday, A. Tuncer, A. Kumbhar, and I. Guvenc, "Improved throughput coverage in natural disasters: Unmanned aerial base stations for public-safety communications," *IEEE Veh. Technol. Mag.*, vol. 11, no. 4, pp. 53–60, Dec. 2016.

[16] R. I. Bor-Yaliniz, A. El-Keyi, and H. Yanikomeroglu, "Efficient 3-D placement of an aerial base station in next generation cellular networks," in *Proc. ICC*, May 2016, pp. 1–5.

[17] I. Bor-Yaliniz and H. Yanikomeroglu, "The new frontier in RAN heterogeneity: Multi-tier drone-cells," *IEEE Commun. Mag.*, vol. 54, no. 11, pp. 48–55, Nov. 2016.

[18] E. Kalantari, H. Yanikomeroglu, and A. Yongacoglu, "On the number and 3D placement of drone base stations in wireless cellular networks," in *Proc. IEEE VTC-Fall*, Sep. 2016, pp. 1–6.

[19] M. Helmy, Z. E. Ankarali, M. Siala, T. Baykas, and H. Arslan, "Dynamic utilization of low-altitude platforms in aerial heterogeneous cellular networks," in *Proc. IEEE Wireless Microw. Technol. Conf. (WAMICON)*, Apr. 2017, pp. 1–6.

[20] E. Kalantari, M. Z. Shakir, H. Yanikomeroglu, and A. Yongacoglu, "Backhaul-aware robust 3D drone placement in 5G+ wireless networks," in *Proc. ICC Workshops*, May 2017, pp. 109–114.

[21] M. Alzenad, A. El-Keyi, F. Lagum, and H. Yanikomeroglu, "3-D Placement of an unmanned aerial vehicle base station (UAV-BS) for energy-efficient maximal coverage," *IEEE Wireless Commun. Lett.*, vol. 6, no. 4, pp. 434–437, Aug. 2017.

[22] M. Mozaffari, W. Saad, M. Bennis, and M. Debbah, "Efficient deployment of multiple unmanned aerial vehicles for optimal wireless coverage," *IEEE Commun. Lett.*, vol. 20, no. 8, pp. 1647–1650, Aug. 2016.

[23] Q. Wu, Y. Zeng, and R. Zhang, "Joint trajectory and communication design for multi-UAV enabled wireless networks," *IEEE Trans. Wireless Commun.*, vol. 17, no. 3, pp. 2109–2121, Mar. 2018.

[24] W. Shi *et al.*, "3D multi-drone-cell trajectory design for efficient IoT data collection," in *Proc. IEEE ICC*, May 2019, pp. 1–6.

[25] W. Shi *et al.*, "Multi-drone 3-D trajectory planning and scheduling in drone-assisted radio access networks," *IEEE Trans. Veh. Technol.*, vol. 68, no. 8, pp. 8145–8158, Aug. 2019.

[26] M. Chen, M. Mozaffari, W. Saad, C. Yin, M. Debbah, and C. S. Hong, "Caching in the sky: Proactive deployment of cache-enabled unmanned aerial vehicles for optimized quality-of-experience," *IEEE J. Sel. Areas Commun.*, vol. 35, no. 5, pp. 1046–1061, May 2017.

[27] M. Chen, W. Saad, and C. Yin, "Liquid state machine learning for resource and cache management in LTE-U unmanned aerial vehicle (UAV) networks," *IEEE Trans. Wireless Commun.*, vol. 18, no. 3, pp. 1504–1517, Mar. 2019.

[28] S.-F. Chou, Y.-J. Yu, A.-C. Pang, and T.-A. Lin, "Energy-aware 3D aerial small-cell deployment over next generation cellular networks," in *Proc. IEEE VTC-Spring*, Jun. 2018, pp. 1–5.

[29] A. Al-Hourani, S. Kandeepan, and A. Jamalipour, "Modeling air-to-ground path loss for low altitude platforms in urban environments," in *Proc. GLOBECOM*, Dec. 2014, pp. 2898–2904.

[30] NGMN Alliance. (Jun. 2012). *Small Cell Backhaul Requirements*. [Online]. Available: https://www.ngmn.org/publications/ngmn-whitepapersmall-cell-backhaul-requirements.html.

[31] *Connecting the World From the Sky*, Facebook, Menlo Park, CA, USA, Mar. 2014.

[32] R. Ghanavi, E. Kalantari, M. Sabbaghian, H. Yanikomeroglu, and A. Yongacoglu, "Efficient 3D aerial base station placement considering users mobility by reinforcement learning," *IEEE WCNC*, Apr. 2018, pp. 1–6.

[33] Federal Aviation Administration. (Jul. 2017). *Fly for Fun Under the Special Rule for Model Aircraft*. [Online]. Available: https://www.faa.gov/uas/getting_started/fly_for_fun/

[34] S. Boyd and L. Vandenberghe, *Convex Optimization*. Cambridge, U.K.: Cambridge Univ. Press, Mar. 2004.

[35] S. Boyd, L. Xiao, and A. Mutapcic, "Subgradient methods," Stanford Univ., Stanford, CA, USA, Lecture Notes EE392o, Oct. 2003.

[36] K. G. Murty and S. N. Kabadi, "Some np-complete problems in quadratic and nonlinear programming," *Math. Program.*, vol. 39, no. 2, pp. 117–129, Jun. 1987.

[37] Y.-Z. Lu, Y.-W. Chen, M.-R. Chen, P. Chen, and G.-Q. Zeng, *Extremal Optimization: Fundamentals, Algorithms, and Applications*. Boca Raton, FL, USA: Auerbach Publications, 2016.

[38] S. Vhaduri and C. Poellabauer, "Hierarchical cooperative discovery of personal places from location traces," *IEEE Trans. Mobile Comput.*, vol. 17, no. 8, pp. 1865–1878, Aug. 2018.

[39] Y. Han, J. Yao, X. Lin, and L. Wang, "GALLOP: Global feature fused location prediction for different check-in scenarios," *IEEE Trans. Knowl. Data Eng.*, vol. 29, no. 9, pp. 1874–1887, Sep. 2017.

[40] M. Asadpour, B. V. den Bergh, D. Giustiniano, K. A. Hummel, S. Pollin, and B. Plattner, "Micro aerial vehicle networks: An experimental analysis of challenges and opportunities," *IEEE Commun. Mag.*, vol. 52, no. 7, pp. 141–149, Jul. 2014.

[41] Y. Zhou, N. Cheng, N. Lu, and X. S. Shen, "Multi-UAV-aided networks: Aerial-ground cooperative vehicular networking architecture," *IEEE Veh. Technol. Mag.*, vol. 10, no. 4, pp. 36–44, Dec. 2015.

[42] *Further Advancements for E-UTRA Physical Layer Aspects*, document TR 36.814, Version 9.0.0, 3GPP, Mar. 2010.

[43] X. Ge, J. Ye, Y. Yang, and Q. Li, "User mobility evaluation for 5G small cell networks based on individual mobility model," *IEEE J. Sel. Areas Commun.*, vol. 34, no. 3, pp. 528–541, Mar. 2016.

Shih-Fan Chou received the double B.S. degree from the Department of Computer Science and the Department of Management Science, National Chiao Tung University, Hsinchu, Taiwan, in 2009, the M.S. degree from the Institute of Network Engineering, National Chiao Tung University, in 2011, and the Ph.D. degree from the Department of Computer Science and Information Engineering, National Taiwan University, Taipei, Taiwan, in 2017. She is currently a Post-Doctoral Fellow with the Research Center for Information Technology Innovation, Academia Sinica, Taipei. Her primary research interests include mobile communications and broadband cellular networks. She was a recipient of the Google Anita Borg Memorial Scholarship in 2013.

Authorized licensed use limited to: Korea Univ. Downloaded on February 13,2020 at 05:48:36 UTC from IEEE Xplore. Restrictions apply.

Ai-Chun Pang received the B.S., M.S., and Ph.D. degrees in computer science and information engineering from National Chiao Tung University, Taiwan, in 1996, 1998, and 2002, respectively. She joined the Department of Computer Science and Information Engineering, National Taiwan University (NTU), Taiwan, in 2002, where she is currently a Professor and the Associate Dean with the College of Electrical Engineering and Computer Science. She was the Director of the Graduate Institute of Networking and Multimedia from 2013 to 2016. She is also an Adjunct Professor with the Graduate Institute of Communication Engineering, NTU, and an Adjunct Research Fellow with the Research Center for Information Technology Innovation, Academia Sinica, Taiwan. Her research interests include mobile communications, software defined networking, and fog/edge computing for the next-generation IoT services.

Ya-Ju Yu received the B.S. degree in computer and communication engineering from the National Kaohsiung First University of Science and Technology, Kaohsiung, Taiwan, in 2005, the M.S. degree in communication engineering from National Central University, Taoyuan, Taiwan, in 2007, and the Ph.D. degree from the Graduate Institute of Networking and Multimedia, National Taiwan University, Taipei, Taiwan, in 2012. He is currently an Assistant Professor with the Department of Computer Science and Information Engineering, National University of Kaohsiung, Kaohsiung. His research interests include the narrowband Internet of Things (NB-IoT), multimedia communications, and wireless mobile networks.

Authorized licensed use limited to: Korea Univ. Downloaded on February 13,2020 at 05:48:36 UTC from IEEE Xplore. Restrictions apply.